Solid State Nuclear Magnetic Resonance 72 (2015) 118–126

Contents lists available at ScienceDirect

Solid State Nuclear Magnetic Resonance

journal homepage: www.elsevier.com/locate/ssnmr

Aromatic spectral editing techniques for magic-angle-spinning solid-state NMR spectroscopy of uniformly ^{13}C-labeled proteins

Jonathan K. Williams [a], Klaus Schmidt-Rohr [b], Mei Hong [a,*]

[a] Department of Chemistry, Massachusetts Institute of Technology, Cambridge, MA 02139, United States
[b] Department of Chemistry, Brandeis University, Waltham, MA 02453, United States

ARTICLE INFO

Article history:
Received 3 July 2015
Received in revised form
8 September 2015
Accepted 11 September 2015
Available online 14 September 2015

Keywords:
Aromatic residues
Gated decoupling
ASSET
PDSD

ABSTRACT

The four aromatic amino acids in proteins, namely histidine, phenylalanine, tyrosine, and tryptophan, have strongly overlapping ^{13}C chemical shift ranges between 100 and 160 ppm, and have so far been largely neglected in solid-state NMR determination of protein structures. Yet aromatic residues play important roles in biology through π–π and cation–π interactions. To better resolve and assign aromatic residues' ^{13}C signals in magic-angle-spinning (MAS) solid-state NMR spectra, we introduce two spectral editing techniques. The first method uses gated ^{1}H decoupling in a proton-driven spin-diffusion (PDSD) experiment to remove all protonated ^{13}C signals and retain only non-protonated carbon signals in the aromatic region of the ^{13}C spectra. The second technique uses chemical shift filters and ^{1}H–^{13}C dipolar dephasing to selectively detect the Cα, Cβ and CO cross peaks of aromatic residues while suppressing the signals of all aliphatic residues. We demonstrate these two techniques on amino acids, a model peptide, and the microcrystalline protein GB1, and show that they significantly simplify the 2D NMR spectra and both reveal and permit the ready assignment of the aromatic residues' signals.

1. Introduction

Spectral overlap in solid-state NMR MAS spectra remains a challenge in structure determination of proteins and other biological macromolecules. While 2D and 3D correlation experiments are now routinely employed in structure determination [1–7], for dynamically or statically disordered or conformationally polymorphic proteins, the ^{13}C and ^{15}N linewidths often exceed 1 ppm [8], which make even 3D correlation spectroscopy often insufficient for complete resolution of the signals except for the smallest proteins [9]. A number of strategies have been proposed to address this challenge. Optimized sample preparation methods can produce conformational homogeneity, although the biological relevance of the selected conformation is usually unclear. Sparse isotopic labeling [10–13] and segmental labeling based on chemical ligation [14] decrease the complexity of the NMR spectra and thus increase the reliability of the assignment, but they contain less information per spectrum. Semi-automated resonance assignment protocols have been designed to explicitly address ambiguities in resonance assignment of broad-line spectra [15–18], but do not indicate to what extent the assignment ambiguity is due to incomplete information or due to structural polymorphism.

Spectral editing is a complementary approach to simplify and resolve protein solid-state NMR spectra without requiring the production of multiple samples. Spectral editing was first developed for natural abundance organic compounds. Opella and Frey described a modification of the 1D cross polarization (CP)-MAS experiment that selectively detects non-protonated ^{13}C signals by inserting a period without ^{1}H decoupling [19]. Zilm and coworkers distinguished between and assigned CH, CH_2 and CH_3 groups by combining CP with polarization inversion and depolarization, taking advantage of different polarization transfer rates of the differently protonated carbons [20–22]. Schmidt-Rohr and coworkers developed various spectral editing methods based on chemical shift filtering [23–25], multiple-quantum dipolar transfer [26,27], and dipolar dephasing [23,25] to separate and assign overlapping resonances in complex organic materials, such as soil organic matter and carbon materials.

Recently, spectral editing has also been introduced to facilitate the structure determination of uniformly ^{13}C, ^{15}N-labeled proteins. We showed how to selectively detect CH-containing Val, Leu and Ile signals using a dipolar DEPT (distortionless enhancement by polarization transfer) technique, distinguish carboxyl-containing Asp and Glu sidechains from amides by asymmetric ^{13}C^{15}N REDOR, and selectively detect dynamic residues by gated ^{1}H decoupling [28]. In addition to spectral editing based on chemical structure and molecular motion, differences in the Cα chemical shift anisotropies (CSAs) and backbone ϕ torsion angle between β-strand

* Corresponding author.
E-mail address: meihong@mit.edu (M. Hong).

http://dx.doi.org/10.1016/j.ssnmr.2015.09.006
0926-2040/

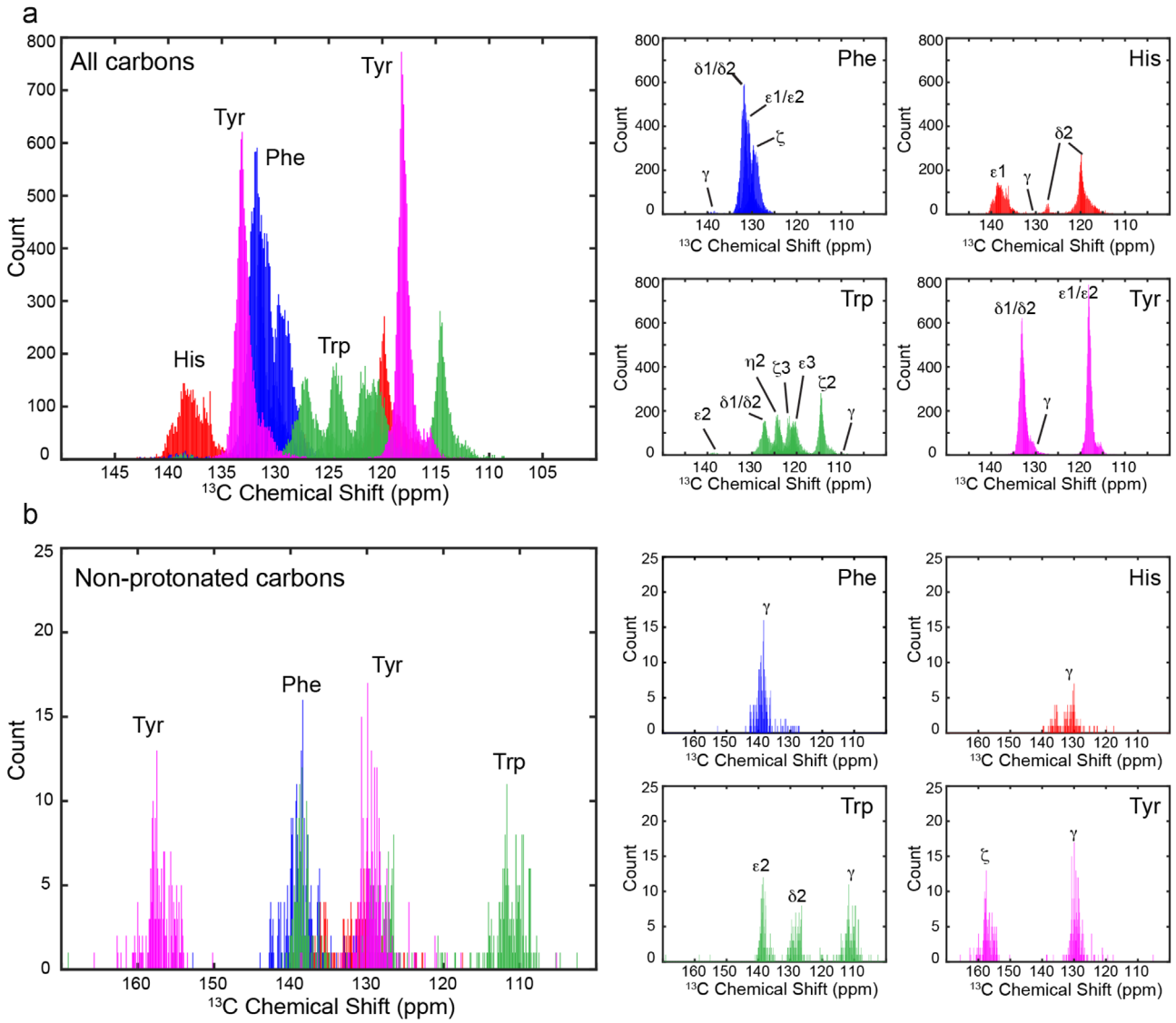

Fig. 1. ^{13}C chemical shift distributions of the four aromatic residues in proteins from the Biological Magnetic Resonance Data Bank. A large degree of resonance overlap exists in the 110–140 ppm region. (a) All aromatic ^{13}C signals. (b) Only non-protonated aromatic ^{13}C signals. Small panels on the right show the chemical shift dispersions of the individual amino acids.

and α-helical residues have been exploited to simplify 2D correlation spectra and selectively detect helical or strand residues [29,30]. Similarly, another structural property, which is the differential water contact of protein residues, has been used to edit the spectra of membrane proteins [8,31–33].

However, so far most protein spectral editing techniques target aliphatic residues, and no methods are yet available to enhance the resolution of aromatic residues. Trp, His, Tyr and Phe play important roles in biology through π–π and cation–π interactions among themselves and with polar residues [34–36] and by functionally relevant ring motions [37,38]. Trp is also well known to stabilize membrane protein structure and topology by acting as an anchoring residue at the membrane-water interface [39]. Aromatic carbons in these four amino acids largely resonate between 140 and 100 ppm, giving rise to a highly congested spectral region. Fig. 1 shows the ^{13}C chemical shift distribution, extracted from the BMRB database [40], of 23 aromatic carbons in proteins. For residue-type assignment, the only well resolved signals are the non-protonated Tyr Cζ peak at ~158 ppm and to some extent the Trp Cγ signal at ~110 ppm, which occupy the outer limits of the aromatic chemical shift range. The other non-protonated carbons, including Phe Cγ, Tyr Cγ, His Cγ, Trp Cδ2 and Trp Cε2, resonate between 140 and 130 ppm. For histidine, the protonation state of the sidechain significantly affects the ^{13}C chemical shifts [41], causing the non-protonated Cγ chemical shift to vary between 128 and 138 ppm.

Two other factors that complicate the assignment of aromatic ^{13}C signals are their large CSAs and the difficulty of avoiding rotational-resonance (R^2) [42] line broadening that arises when the chemical-shift difference matches the MAS frequency ν_r or $2\nu_r$ ($n=1$ and $n=2$ R^2 condition). The large aromatic ^{13}C CSAs give rise to spinning sidebands in the spectra that usually extend into the aliphatic region. More insidiously, the Cβ and Cγ isotropic chemical shift differences of aromatic residues are typically 80–100 ppm [15], which fall between the $n=1$ and $n=2$ R^2 conditions of 120 ppm and 60 ppm for backbone Cα and CO chemical shifts, respectively. Thus, MAS frequencies are often accidentally close to some of the aromatic residues' Cβ and Cγ isotropic shift differences, broadening both peaks. Fig. 2a shows the ^{13}C CP-MAS spectra of uniformly ^{13}C, ^{15}N-labeled Trp under 4–12 kHz MAS at 1 kHz intervals. At the ^{13}C Larmor frequency of 100 MHz used to measure these spectra, these MAS frequencies correspond to 40–

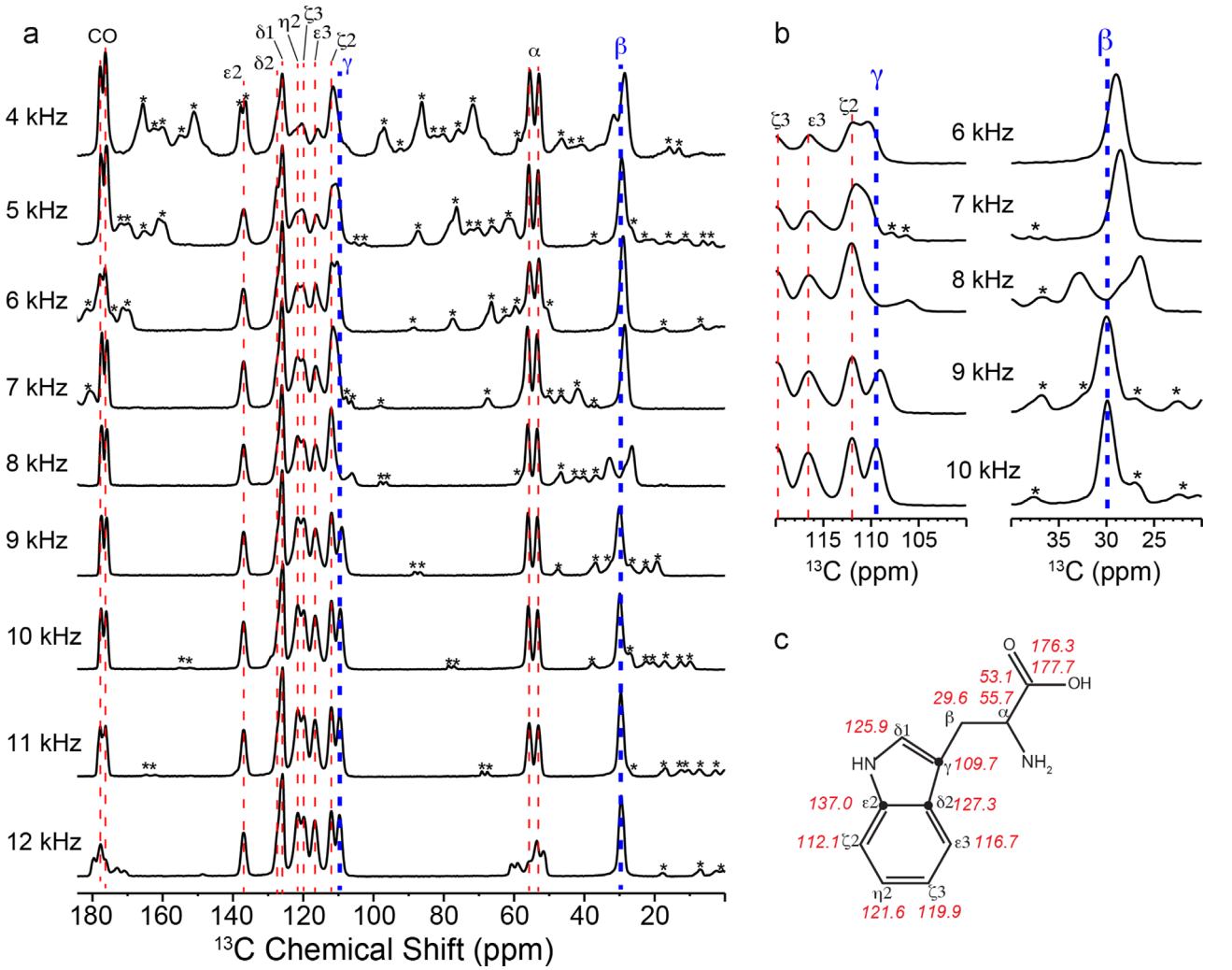

Fig. 2. 1D CP-MAS spectra of U–^{13}C,^{15}N labeled Trp as a function of MAS frequency. (a) Full 1D spectra measured in a 9.4 T magnetic field, corresponding to 100 MHz ^{13}C Larmor frequency. At 8 kHz (80 ppm) and 12 kHz (120 ppm) MAS frequencies, rotational resonance broadening is observed for the Cβ–Cγ spin pair and the Cα–CO spin pair, respectively. (b) Expanded Cγ and Cβ regions of the ^{13}C spectra, showing R^2-induced line broadening. MAS frequencies that are within 1 kHz (or 10 ppm) of the R^2 conditions are insufficient for removing line broadening. In all panels, spinning sidebands are marked with an asterisk. (c) Accurate ^{13}C isotropic shifts of Trp, obtained from the 11 kHz MAS spectrum, which is free of R^2 effects and spinning sideband overlap.

120 ppm. The Cγ and Cβ isotropic shift difference for Trp is 80.1 ppm, which gives an $n=1$ R^2 condition of 8 kHz (80 ppm) MAS and an $n=2$ R^2 condition of 4 kHz (40 ppm) MAS. Thus, the Cγ and Cβ peaks are split and broadened at 4 kHz and 8 kHz MAS, as well as within 1 kHz windows of these two frequencies (Fig. 2b). Moreover, at MAS frequencies lower than 6 kHz (or 60 ppm), significant aromatic sidebands exist that overlap with the aliphatic signals. Under 12 kHz (or 120 ppm) MAS, the CO and Cα peaks are severely split by the R^2 effect. These multiple R^2 conditions restrict the choice of MAS frequencies to 11 kHz (or 110 ppm) for Trp, which gives the best compromise of avoiding R^2 broadening as well as minimizing spinning sidebands (Fig. 2a and b). For uniformly ^{13}C-labeled proteins with multiple aromatic residues, choosing an appropriate MAS frequency that avoids all R^2 conditions is thus crucial for minimizing mis-assignment of aromatic residues' Cβ and Cγ signals.

In this study, we describe two techniques for reducing spectral overlap and facilitating assignment of the ^{13}C signals of aromatic residues in proteins. The first technique is a simple modification of the 2D ^{13}C–^{13}C PDSD experiment to include a gated ^{1}H decoupling period before direct detection. The resulting 2D PDSD spectrum correlates all ^{13}C signals in the indirect dimension with only the signals of non-protonated carbons in the direct dimension. The second technique is designed to suppress all Cα–Cβ cross peaks of aliphatic residues, leaving only the Cα, Cβ and CO cross peaks of aromatic residues. The Cα and Cβ magnetization of all residues is first removed by chemical shift filters and ^{13}C–^{1}H dipolar filters, then the remaining aromatic ^{13}C magnetization is transferred to the Cα, Cβ and CO of only the aromatic residues by a short spin diffusion period. We demonstrate these two techniques on amino acids, a model peptide, and the microcrystalline model protein GB1.

2. Experimental conditions

Solid-state NMR experiments were carried out on Bruker 400 MHz (9.4 T) and 800 MHz (18.8 T) spectrometers using 4 mm or 3.2 mm MAS probes. The samples were spun at frequencies between 4.0 kHz and 16.5 kHz. Typical radiofrequency field strengths were 71–83 kHz for ^{1}H and 50–71 kHz for ^{13}C. ^{13}C chemical shifts were referenced to the CH_2 peak of adamantane at 38.48 ppm on the TMS scale [43]. Four uniformly ^{13}C and ^{15}N labeled model compounds were used to test the pulse sequences: the amino acid Trp, a five-amino-acid mixture, WYIEN, the tripeptide formyl-Met-Leu-Phe (MLF) [2,44,45], and the

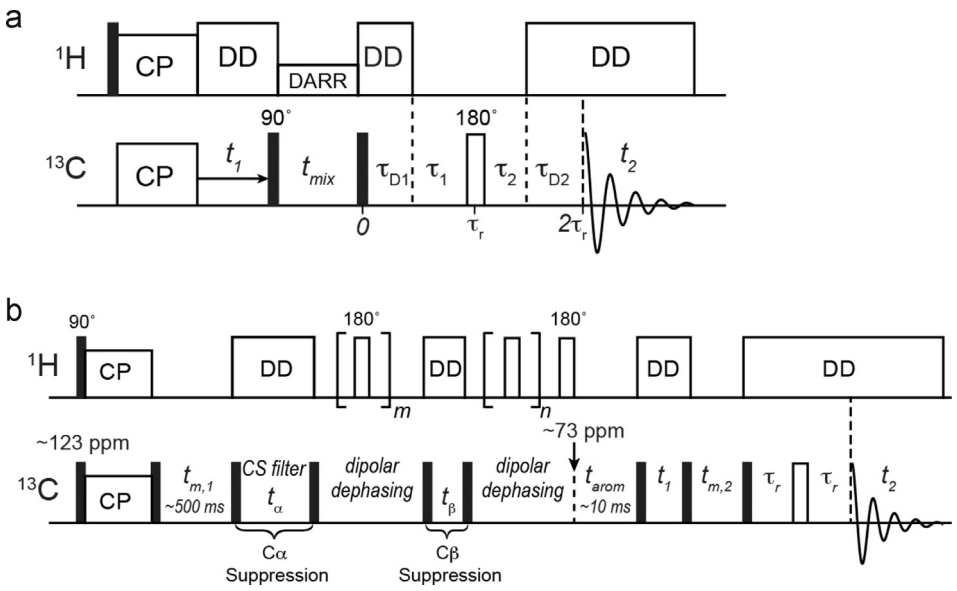

Fig. 3. Pulse sequences developed in this work. (a) 2D PDSD with gated ^{1}H decoupling. The gated decoupling period contains $\tau_1 = 60$ μs and $\tau_2 = 40$ μs for the MAS frequencies used in this work. (b) 2D *A*romatic *S*election by *S*pectral *E*diting (ASSET). The initial spin diffusion period is set relatively long ($t_{m,1} = 500$ ms) to ensure polarization of aromatic side chains. This is followed by two chemical shift filters, one for Cα suppression (t_α) and one for Cβ suppression (t_β). Each chemical shift filter is followed by a ^{13}C–^{1}H dipolar recoupled z-filter period to destroy the transverse magnetization of other aliphatic carbons that are far off-resonance from the aromatic region. A spin diffusion period, t_{arom}, then transfers the remaining aromatic ^{13}C magnetization to the Cβ and Cα of the aromatic residues. 2D correlation of Cβ and Cα resonances is then conducted using a typical PDSD module with Hahn echo detection.

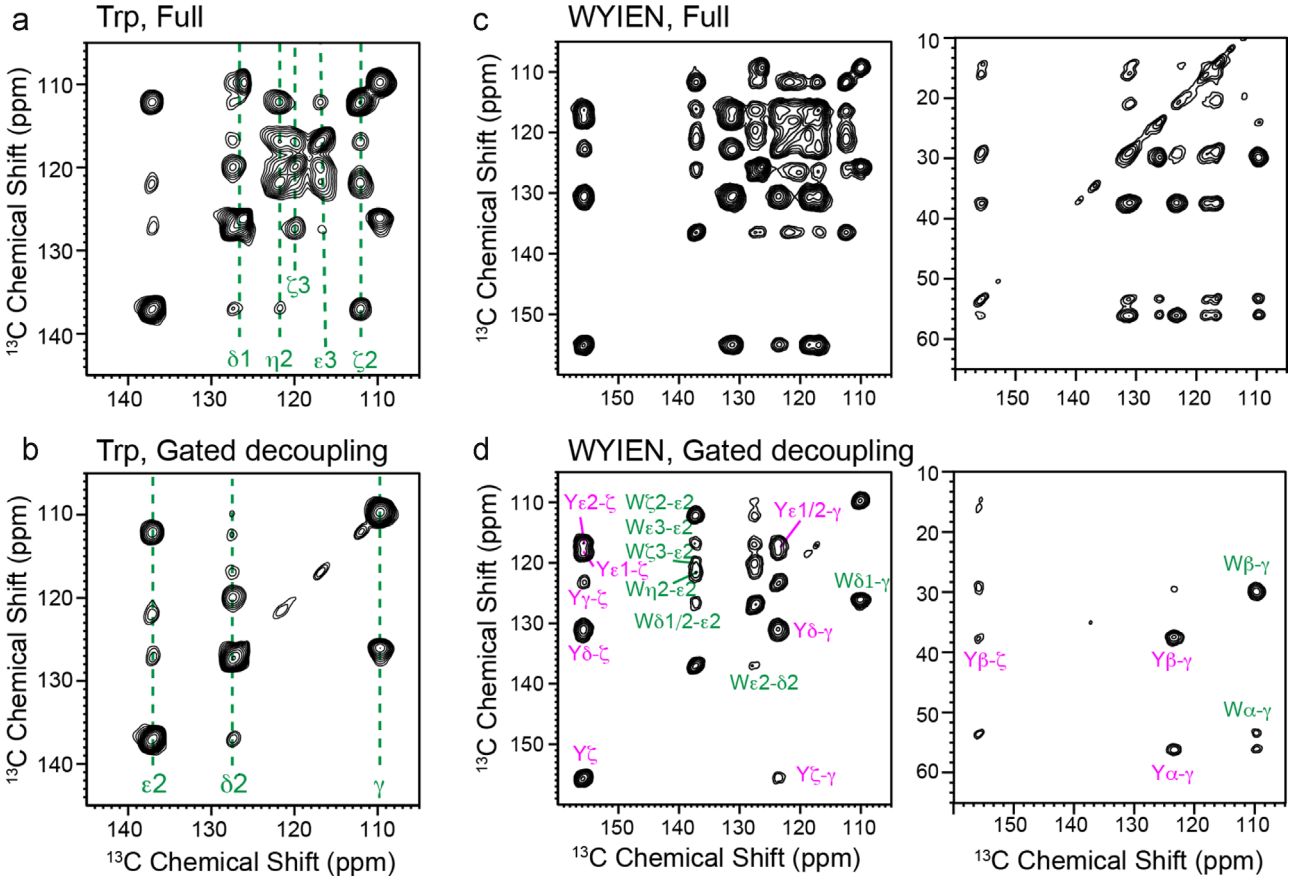

Fig. 4. 2D ^{13}C–^{13}C DARR (top) and gPDSD (bottom) spectra of U–^{13}C Trp (a, b) and the amino acid mixture WYIEN (c, d). Spectra (a) and (b) were recorded under 11 kHz MAS using a mixing time of 2 ms and ^{1}H gate times of $\tau_1 = 60$ μs and $\tau_2 = 40$ μs. Spectra (c) and (d) were measured under 10.3 kHz MAS using a mixing time of 10 ms and ^{1}H gate times of $\tau_1 = 60$ μs and $\tau_2 = 40$ μs. The aromatic region in (b) and (d) retains only the non-protonated ^{13}C signals in the direct dimension. For the amino acid mixture, the aliphatic–aromatic correlation region is also simplified after removal of the protonated aromatic ^{13}C signals, facilitating assignment of the Cβ and Cα chemical shifts of Tyr and Trp.

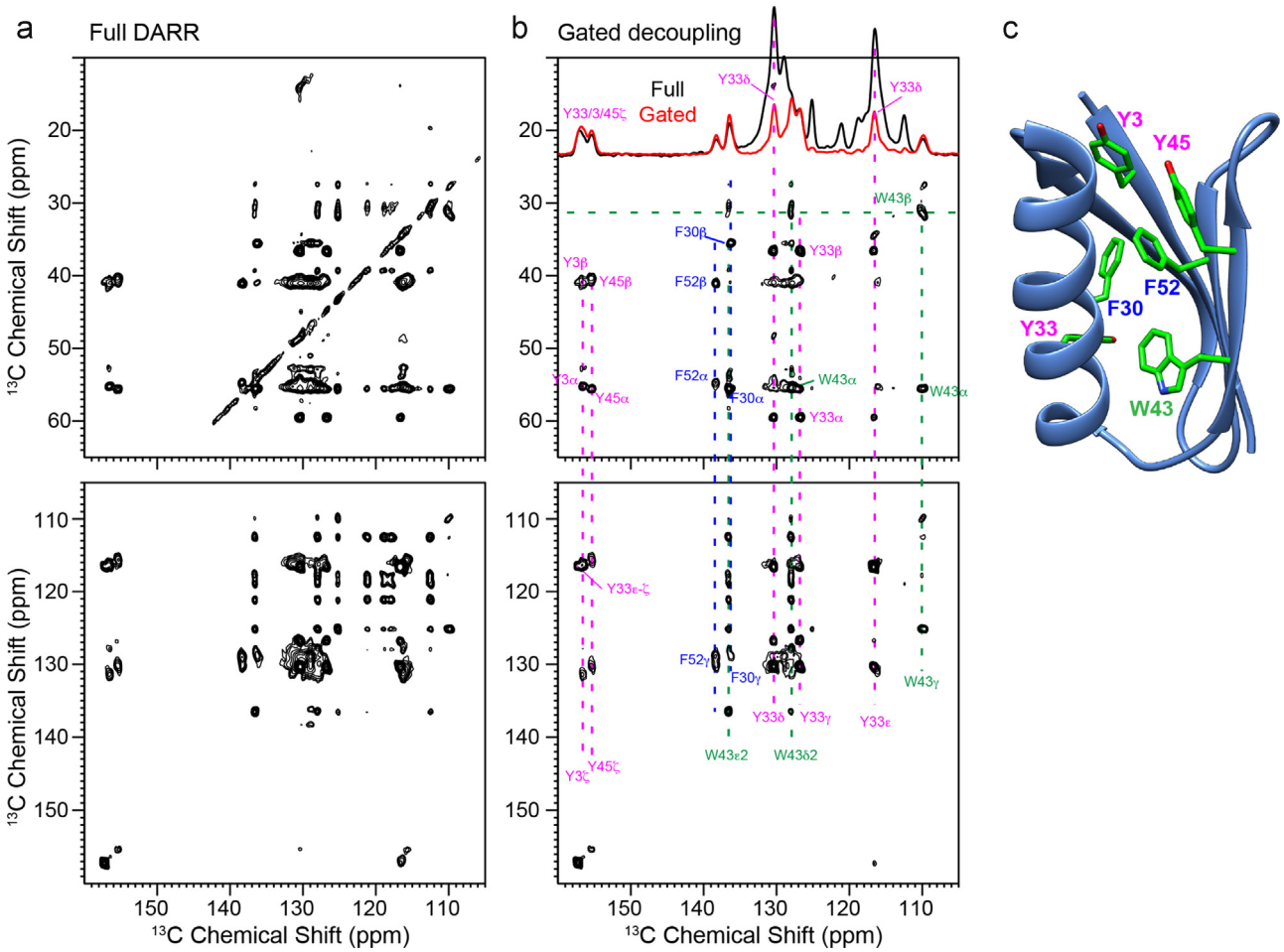

Fig. 5. 2D ^{13}C PDSD (a) and gPDSD (b) spectra of GB1 measured at 18.8 T (800 ^{1}H Larmor frequency) under 16.5 kHz MAS with a mixing time of 100 ms. ^{1}H gate times of τ_1= 36 μs and τ_2=24 μs were used for spectra (b). (c) GB1 structure (PDB: 2QMT) showing the positions of the six aromatic residues.

microcrystalline protein GB1. These model systems provide increasing levels of complexity for spectral editing, culminating in GB1, which contains six aromatic residues out of a total of 56 residues [46].

3. Pulse sequences

3.1. ^{1}H gated decoupling PDSD (gPDSD) experiment

The conventional 2D PDSD experiment gives ^{13}C–^{13}C correlation peaks within an amino acid residue at short mixing times and both short and long-range correlations at long mixing times. With a T_1-relaxation compensation scheme, difference spectra showing only long-range cross peaks can also be obtained [47]. To detect only non-protonated aromatic ^{13}C signals in the aromatic region of the PDSD spectrum, we add a ^{1}H gated decoupling period after the spin diffusion mixing time and before t_2 detection (Fig. 3a). The gate during which ^{1}H decoupling is turned off consists of a total delay of $\tau_1+\tau_2$, which spans part of two rotor periods. They are demarcated by a ^{13}C 180° pulse on the rotor echo to refocus the ^{13}C chemical shift, and also recouple the ^{13}C–^{1}H dipolar coupling to better dephase the ^{13}C magnetization. The remaining periods during which ^{1}H decoupling is on are τ_{D1} and τ_{D2}, where $\tau_{D1}+\tau_1$ and $\tau_2+\tau_{D2}$ equal one rotor period. τ_1 and τ_2 are in general not the same. In the current work, under 10.3 kHz MAS, we found that the optimal delays for maximal dephasing of the protonated aromatic signals are τ_1=60 μs and τ_2=40 μs.

3.2. Aromatic selection via spectral editing (ASSET) experiment

Fig. 3b shows the pulse sequence for obtaining only aromatic Cα–Cβ cross peaks in the aliphatic region of the 2D PDSD spectra. At the beginning of the pulse sequence, the ^{13}C carrier frequency is set in the middle of the aromatic region, around 123 ppm. A ^{13}C 90° pulse together with ^{1}H–^{13}C CP allow the detection of both dynamic and rigid functional groups. A subsequent spin diffusion period, $t_{m,1}$, of ~500 ms further enhances the aromatic ^{13}C intensities by equilibrating the aliphatic and aromatic ^{13}C magnetization, since the low proton density of aromatic residues causes lower signals in a conventional ^{13}C CP spectrum [25]. After the pre-equilibration period, a 90° pulse flips all ^{13}C magnetization to the transverse plane, where chemical shift evolution with aromatic residues on or near resonance is allowed to occur for a period t_α, which alternates between 0 and a finite time that creates antiparallel magnetization vectors between Cα and aromatic carbons. For experiments at a ^{13}C Larmor frequency of 100 MHz (9.4 T), the best t_α is 0 and 83 μs. A subsequent 90° pulse with suitable phase cycling every two scans then stores the aromatic ^{13}C magnetization along $+z$ while the Cα magnetization alternates between $+z$ and $-z$. Any transverse magnetization is then dephased by ^{13}C–^{1}H dipolar coupling, which is recoupled using a ^{1}H 180° pulse every half rotor period. After this z-filter, the stored ^{13}C z-magnetization is returned to the transverse plane by another 90° pulse, and a similar chemical shift filter together with a z-filter is used to destroy the Cβ magnetization. At 100 MHz ^{13}C Larmor frequency, the optimal Cβ chemical shift filter time, t_β, is 0 and

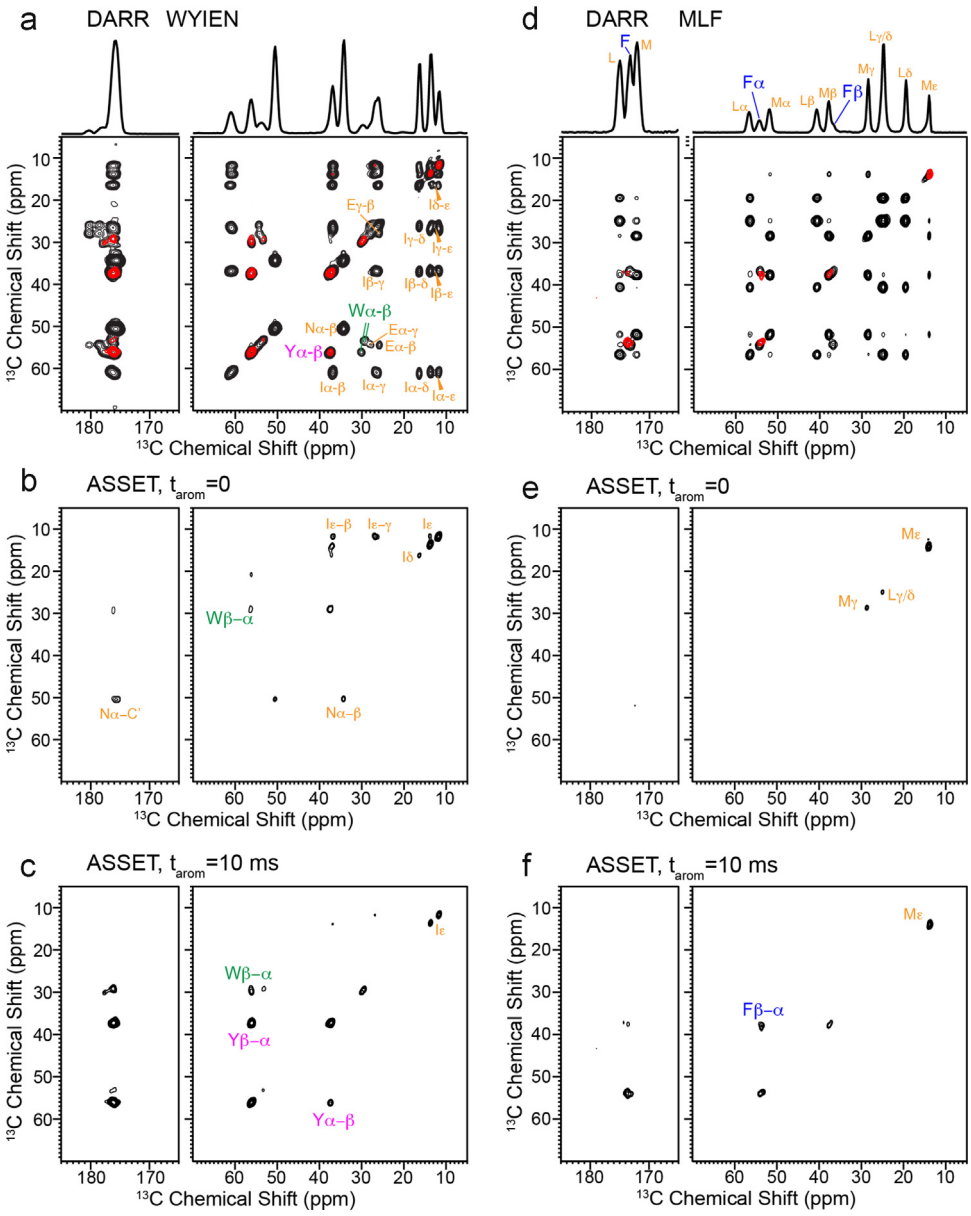

Fig. 6. 2D ^{13}C–^{13}C DARR and ASSET spectra of the amino acid mixture WYIEN (a–c) and tripeptide MLF (D–f). (a, d) Full DARR spectra showing all cross peaks. (b, e) Spectra with $t_{arom}=0$, where most Cα and Cβ cross peaks are suppressed. (c, f) ASSET spectra with $t_{arom}=10$ ms, which exhibit mostly aromatic Cα and Cβ cross peaks. The spectra in (c) and (f) are reproduced in red in (a) and (d) to compare with the full DARR spectra.

47 μs. Due to the sufficiently high MAS frequency, t_α and t_β need not be rotor-synchronized. The z-filter periods can also have different lengths, and were optimized to be 2 and 4 rotor periods at an MAS frequency of ~10 kHz. At this point, the remaining ^{13}C magnetization is mostly aromatic, and is allowed to re-polarize the adjacent Cβ and Cα during a t_{arom} period of 5–25 ms. The ^{13}C carrier frequency is moved to ~73 ppm at the beginning of the t_{arom} period to keep potential zero-frequency artifacts outside the relevant spectral region and avoid significant off-resonance effects. This is followed by a standard 2D PDSD module with a mixing time of $t_{m,2}$, with optional echo detection.

4. Results and discussion

We demonstrate these two spectral editing techniques on several model compounds. Fig. 4a and c shows the full 2D PDSD spectra of Trp and WYIEN, where all intra-residue cross-peaks can be assigned. The gPDSD spectra show a greatly simplified aromatic region. For Trp, all protonated ^{13}C signals are removed in the direct dimension, leaving only cross-peaks of the indole Cγ, Cδ2 and Cε2 (Fig. 4b). For the amino-acid mixture, Trp Cε2, Cδ2 and Cγ and Tyr Cγ and Cζ signals are retained with efficiencies of 42–75% compared to the full spectrum while the protonated aromatic carbons are suppressed to 0–9% of the full intensity (Fig. 4d). In the aliphatic–aliphatic region of the 2D gPDSD spectrum (not shown), residual Ile Cδ and Cε methyl signals are also present due to their motionally averaged ^{13}C–^{1}H dipolar couplings, but the intensities are only ~6% of the full signals. In the aliphatic–aromatic correlation region, the suppression of the protonated ^{13}C signals significantly simplified the assignment of the Trp and Tyr Cβ and Cα chemical shifts.

The gated-decoupling sequence similarly simplified the aromatic region of the GB1 2D spectrum (Fig. 5a and b). Although the high resolution afforded by the 800 MHz spectrometer allowed us to resolve many aromatic ^{13}C peaks of the three Tyr residues (Y3,

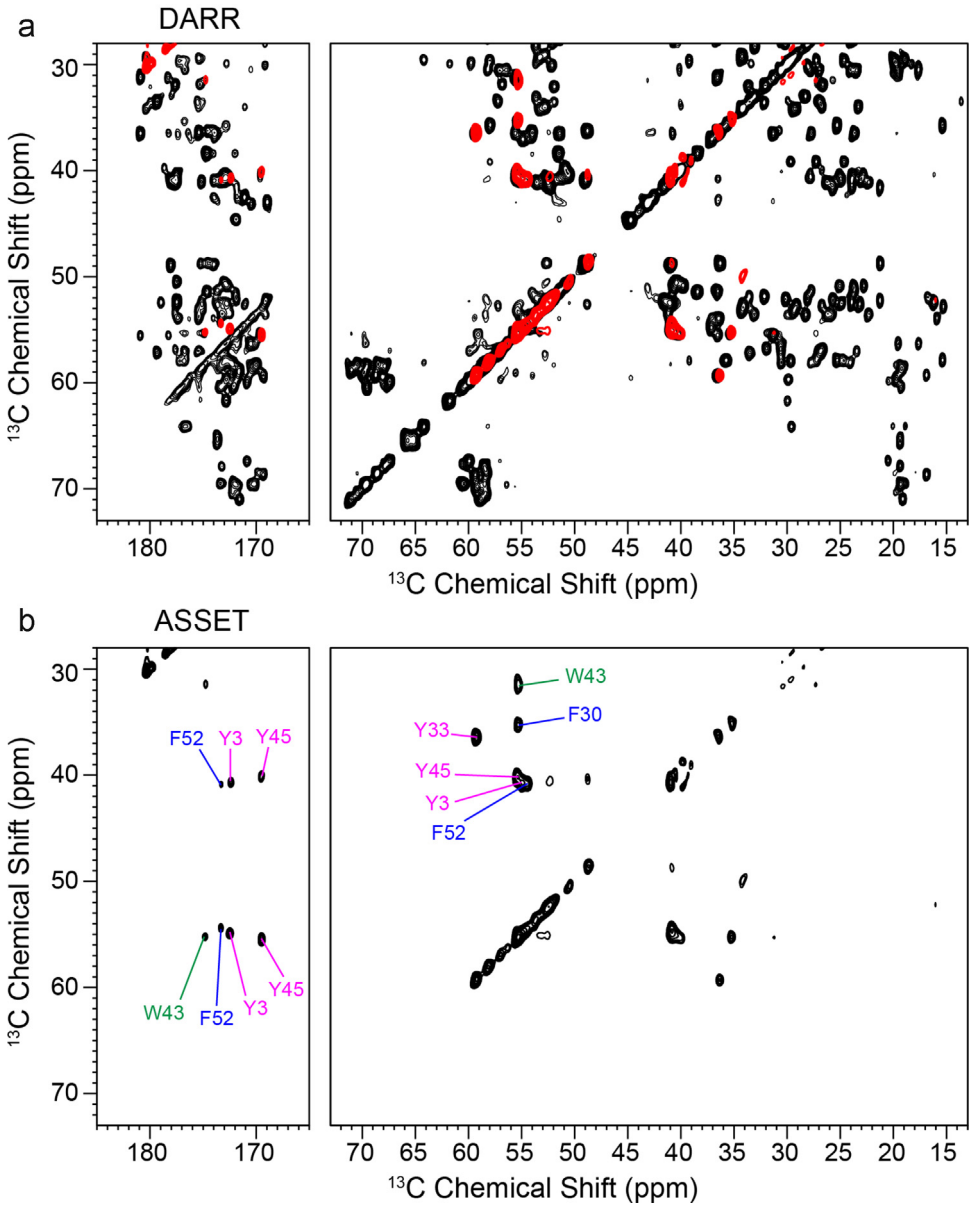

Fig. 7. 2D ^{13}C DARR (a) and ASSET (b) spectra of GB1. The ASSET spectrum was acquired with t_{arom}=25 ms and shows only the Cα–Cβ and Cα/β-CO cross peaks of the six aromatic residues while suppressing the signals of all aliphatic residues. The ASSET spectrum is reproduced in red in (a) and superimposed on the full PDSD spectrum.

Y33, Y45), two Phe residues (F30, F52) and one Trp (W43) [46], resonance overlap remains among Phe Cδ and Cε and Tyr Cγ and Cδ signals, which cluster around 130 ppm. With gated ^{1}H decoupling, most of the F30 and F52 cross peaks in the 126–133 ppm region are suppressed, revealing the underlying Tyr Cγ and Cδ signals in Fig. 5b. Compared to the regular PDSD spectrum, the non-protonated ^{13}C signals are retained to an average of 86% of the full intensities while the protonated aromatic carbons' signals are suppressed to an average of 18% of the full intensities. The slightly higher residual intensities of the protonated aromatic carbons in GB1 compared to the amino acids can be attributed to two reasons. The WYIEN sample was measured on a 400 MHz spectrometer under 10.3 kHz MAS, while GB1 was measured on a 800 MHz spectrometer under 16.5 kHz MAS. The higher MAS frequency was necessary to avoid overlap between the carbonyl spinning sidebands and the aromatic signals, and the resulting shorter rotor period caused a shorter gate, thus reducing the efficiency of dipolar dephasing. The GB1 gPDSD spectrum was measured using a total gating delay of $\tau_1+\tau_2$=60 μs, while the amino acid mixture was measured with a total delay of 100 μs. The incomplete suppression under faster MAS can be remedied by extending the dipolar dephasing period. In addition, molecular motion, which may be present for the less hydrophobically embedded aromatic residues in GB1, can also reduce the efficiency of gated decoupling. For example, we observe 33% residual intensity of the Tyr Cδ and Tyr Cε peak in the gated decoupling spectrum (Fig. 5b). This can be assigned to one of the three Tyr residues, Y33, which is located on the surface of the protein with its sidechain pointed away from the hydrophobic pore. Indeed, Y33 was found to undergo two-site ring flips [46], which average the ^{13}C–^{1}H dipolar couplings, thus reducing the efficiency of gated decoupling.

While gPDSD simplifies the aromatic region of 2D ^{13}C PDSD spectra, the ASSET technique selectively detects the Cβ–Cα, Cα–Cβ, Cβ–CO and Cα–CO cross peaks of aromatic residues while suppressing those of aliphatic residues. Fig. 6a and d show the full 2D spectra of the WYIEN mixture and the tripeptide MLF. All intra-residue cross peaks are observed for WYIEN with a 20 ms mixing time (Fig. 6a) while intra- and inter-residue correlations are both

observed in MLF with 30 ms mixing (Fig. 6d). When the ASSET technique is applied without the transfer, i.e. $t_{arom}=0$, the aliphatic signals are nearly completely suppressed, except for a few weak methyl signals (Fig. 6b and e) and Asn and Trp Cα–Cβ peaks, which may result from incomplete chemical shift filtering. When the aromatic transfer is turned on ($t_{arom}=10$ ms), the Cα and Cβ signals of Trp and Tyr in the mixture are selectively enhanced, as shown by Cα–Cβ and Cβ–Cα cross peaks on both sides of the diagonal (Fig. 6c and f). These Trp and Tyr cross peaks are 20–40% of the full intensities, compared to the incompletely suppressed Ile sidechain methyl signals, which are ~3% of the full intensities. A similar result is found for MLF. Here, the Phe shows a Cβ–Cα cross peak but not the Cα–Cβ peak, indicating that the 10 ms t_{arom} is sufficiently short that polarization transfer is dominated by the Cγ–Cβ transfer while Cγ–Cα transfer is reduced. Such cross peak asymmetry can be helpful for spectral editing of larger proteins.

Fig. 7 shows the 2D DARR and ASSET spectra of GB1 using a mixing time of 100 ms between the t_1 and t_2 dimensions. The 2D spectra were measured on an 800 MHz spectrometer under 16.5 kHz MAS, and the DARR spectrum (Fig. 7a) exhibits comparable resolution as the published literature [46]. The ASSET sequence dramatically simplified the aliphatic and carbonyl regions of the spectrum (Fig. 7b), displaying only Cα/β-Cβ/α and Cα/β-CO cross peaks of the six aromatic residues with efficiencies of 10–20%. The Cβ–Cα cross peaks of W43, Y33, and F30 are well resolved, while the Cβ–Cα cross peaks of Y3, Y45 and F52 partially overlap. But the latter three residues are well dispersed by their carbonyl chemical shifts. The aliphatic region of the ASSET spectrum has moderate intensity asymmetry, with the Cβ–Cα cross peaks stronger than Cα–Cβ peaks, indicating that the aromatic carbon magnetization is transferred more readily to Cβ than to Cα with the t_{arom} mixing time of 25 ms used here.

5. Conclusions

We have demonstrated two pulse sequences for measuring simplified and higher-resolution 2D ^{13}C–^{13}C correlation spectra of aromatic residues in proteins. The gPDSD technique results in a non-protonated aromatic ^{13}C sub-spectrum in the direct dimension, correlated with all carbons in the indirect dimension. The ASSET technique yields aromatic residues' Cβ, Cα and CO cross peaks while suppressing all aliphatic residues' cross peaks. The efficiency of the gPDSD technique for aromatic carbons is 62–86%, while the protonated ^{13}C signals are suppressed to less than 20% of the original intensities. The efficiency of the ASSET experiment is 20–40% on small molecules and 10–20% on GB1. The lower efficiency of GB1 may be due to the inherent isotropic shift dispersion, which makes the chemical shift filter imperfect. Overall, the selectivity against non-aromatic residues is excellent for both techniques, thus increasing the repertoire of spectral editing techniques for complex and disordered proteins. In principle, the aromatic-residue-only Cα–Cβ sub-spectrum can also be obtained in a 3D ^{13}C–^{13}C–^{13}C correlation experiment [48], provided that the aromatic ^{13}C chemical shifts are reasonably well resolved, but the signal-averaging time for these 3D experiments is significantly longer than for the 2D spectrally edited ASSET experiment.

Acknowledgements

This work is supported by NIH Grant GM088204 to M. H. The authors would like to thank Dr. Robert Silvers for providing the GB1 sample used in this work.

References

[1] M. Hong, Resonance assignment of ^{13}C/^{15}N labeled proteins by two- and three-Dimensional magic-angle-spinning NMR, J. Biomol. NMR 15 (1999) 1–14.
[2] C.M. Rienstra, M. Hohwy, M. Hong, R.G. Griffin, 2D and 3D ^{15}N–^{13}C–^{13}C NMR chemical shift correlation spectroscopy of solids: assignment of MAS spectra of peptides, J. Am. Chem. Soc. 122 (2000) 10979–10990.
[3] M. Baldus, A.T. Petkova, J. Herzfeld, R.G. Griffin, Cross polarization in the tilted frame: assignment and spectral simplification in heteronuclear spin systems, Mol. Phys. 95 (1998) 1197–1207.
[4] G. Comellas, C.M. Rienstra, Protein structure determination by magic-angle spinning solid-state NMR, and insights into the formation, structure, and stability of amyloid fibrils, Annu. Rev. Biophys. 42 (2013) 515–536.
[5] A.E. McDermott, Structure and dynamics of membrane proteins by magic angle spinning solid-state NMR, Annu. Rev. Biophys. 38 (2009) 385–403.
[6] S. Luca, H. Heise, M. Baldus, High-resolution solid-state NMR applied to polypeptides and membrane proteins, Acc. Chem. Res. 36 (2003) 858–865.
[7] M. Hong, Solid-state NMR studies of the structure, dynamics, and assembly of b-sheet membrane peptides and α-helical membrane proteins with antibiotic activities, Acc. Chem. Res. 39 (2006) 176–183.
[8] S.Y. Liao, K.J. Fritzsching, M. Hong, Conformational analysis of the full-length M2 protein of the influenza A virus using solid-state NMR, Protein Sci. 22 (2013) 1623–1638.
[9] R. Tycko, Prospects for resonance assignments in multidimensional solid-state NMR spectra of uniformly labeled proteins, J. Biomol. NMR 22 (1996) 239–251.
[10] M. Hong, Determination of multiple ϕ torsion angles in solid proteins by selective and extensive ^{13}C labeling and two-dimensional solid-state NMR, J. Magn. Reson. 139 (1999) 389–401.
[11] M. Hong, K. Jakes, Selective and extensive ^{13}C labeling of a membrane protein for solid-state NMR investigations, J. Biomol. NMR 14 (1999) 71–74.
[12] A. Loquet, G. Lv, K. Giller, S. Becker, A. Lange, ^{13}C spin dilution for simplified and complete solid-state NMR resonance assignment of insoluble biological assemblies, J. Am. Chem. Soc. 133 (2011) 4722–4725.
[13] F. Castellani, B. vanRossum, A. Diehl, M. Schubert, K. Rehbein, H. Oschkinat, Structure of a protein determined by solid-state magic-angle spinning NMR spectroscopy, Nature 420 (2002) 98–102.
[14] B. Kwon, D. Tietze, P.B. White, S.Y. Liao, M. Hong, Chemical ligation of the influenza M2 protein for solid-state NMR characterization of the cytoplasmic domain structure, Protein Sci. 24 (2015) 1087–1099.
[15] K.J. Fritzsching, Y. Yang, K. Schmidt-Rohr, M. Hong, Practical use of chemical shift databases for protein solid-state NMR: 2D chemical shift maps and amino-acid assignment with secondary-structure information, J. Biomol. NMR 56 (2013) 155–167.
[16] K.N. Hu, W. Qiang, R. Tycko, A general Monte Carlo/simulated annealing algorithm for resonance assignment in NMR of uniformly labeled biopolymers, J. Biomol. NMR 50 (2011) 267–276.
[17] R. Tycko, K.N. Hu, A Monte Carlo/simulated annealing algorithm for sequential resonance assignment in solid state NMR of uniformly labeled proteins with magic-angle spinning, J. Magn. Reson. 205 (2010) 304–314.
[18] Y. Yang, K.J. Fritzsching, M. Hong, Resonance assignment of disordered proteins using a multi-objective non-dominated sorting genetic algorithm, J. Biomol. NMR 57 (2013) 281–296.
[19] S.J. Opella, M.H. Frey, Selection of nonprotonated carbon resonances in solid-state nuclear magnetic resonance, J. Am. Chem. Soc. 101 (1979) 5854–5856.
[20] X. Wu, S.T. Burns, K.W. Zilm, Spectral editing in CPMAS NMR. generating subspectra based on proton multiplicities, J. Magn. Reson. 111 (1994) 29–36.
[21] X.L. Wu, K.W. Zilm, Complete spectral editing in CPMAS NMR, J. Magn. Reson. 102 (1993) 205–213.
[22] X. Wu, S. Zhang, X. Wu, Selective polarization inversion in solid state high-resolution CP MAS NMR, J. Magn. Reson. 77 (1988) 343–347.
[23] J.D. Mao, K. Schmidt-Rohr, Accurate quantification of aromaticity and non-protonated aromatic carbon fraction in natural organic matter by ^{13}C solid-state nuclear magnetic resonance, Environ. Sci. Technol. 38 (2004) 2680–2684.
[24] J.D. Mao, K. Schmidt-Rohr, Separation of aromatic-carbon ^{13}C NMR signals from di-oxygenated alkyl bands by a chemical-shift-anisotropy filter, Solid State Nucl. Magn. Reson. 26 (2004) 36–45.
[25] R.L. Johnson, J.M. Anderson, B.H. Shanks, X. Fang, M. Hong, K. Schmidt-Rohr, Spectrally edited 2D ^{13}C–^{13}C NMR spectra without diagonal ridge for characterizing ^{13}C-enriched low-temperature carbon materials, J. Magn. Reson. 234 (2013) 112–124.
[26] K. Schmidt-Rohr, J.D. Mao, Efficient CH-group selection and identification in ^{13}C solid-state NMR by dipolar DEPT and ^{1}H chemical-shift filtering, J. Am. Chem. Soc. 124 (2002) 13938–13948.
[27] J.-D. Mao, K. Schmidt-Rohr, Methylene spectral editing in solid-state ^{13}C NMR by three-spin coherence selection, J. Magn. Reson. 176 (2005) 1–6.
[28] K. Schmidt-Rohr, K.J. Fritzsching, S.Y. Liao, M. Hong, Spectral editing of two-dimensional magic-angle-spinning solid-state NMR spectra for protein resonance assignment and structure determination, J. Biomol. NMR 54 (2012) 343–353.
[29] M. Hong, Solid-state NMR determination of ^{13}Ca chemical shift anisotropies for the identification of protein secondary structure, J. Am. Chem. Soc. 122 (2000) 3762–3770.
[30] D. Huster, S. Yamaguchi, M. Hong, Efficient β-sheet identification in proteins by solid-state NMR spectroscopy, J. Am. Chem. Soc. 122 (2000) 11320–11327.
[31] C. Ader, R. Schneider, K. Seidel, M. Etzkorn, S. Becker, M. Baldus, Structural

rearrangements of membrane proteins probed by water-edited solid-state NMR spectroscopy, J. Am. Chem. Soc. 131 (2009) 170–176.
[32] K.K. Kumashiro, K. Schmidt-Rohr, O.J. Murphy, K.L. Ouellette, W.A. Cramer, L. K. Thompson, A novel tool for probing membrane protein structure: solid-state NMR with proton spin diffusion and X-nucleus detection, J. Am. Chem. Soc. 120 (1998) 5043–5051.
[33] I.V. Sergeyev, S. Bahri, L.A. Day, A.E. McDermott, Pf1 bacteriophage hydration by magic angle spinning solid-state NMR, J. Chem. Phys. 141 (2014) 22D533.
[34] J.P. Gallivan, D.A. Dougherty, Cation–p interactions in structural biology, Proc. Natl. Acad. Sci. USA 96 (1999) 9459–9464.
[35] S.Y. Liao, Y. Yang, D. Tietze, M. Hong, The influenza M2 cytoplasmic tail changes the proton-exchange equilibria and the backbone conformation of the transmembrane histidine residue to facilitate proton conduction, J. Am. Chem. Soc. 137 (2015) 6067–6077.
[36] J.K. Williams, Y. Zhang, K. Schmidt-Rohr, M. Hong, pH-dependent conformation, dynamics, and aromatic interaction of the gating tryptophan residue of the influenza M2 proton channel from solid-state NMR, Biophys. J. 104 (2013) 1698–1708.
[37] W. Hu, N.D. Lazo, T.A. Cross, Tryptophan dynamics and structural refinement in a lipid bilayer environment: solid state NMR of the Gramicidin channel, Biochemistry 34 (1995) 14138–14146.
[38] C.M. Gall, T.A. Cross, J.A. DiVerdi, S.J. Opella, Protein dynamics by solid-state NMR: aromatic rings of the coat protein in fd bacteriophage, Proc. Natl. Acad. Sci. USA 79 (1982) 101–105.
[39] M.R. de Planque, B.B. Bonev, J.A. Demmers, D.V. Greathouse, R.En Koeppe, F. Separovic, A. Watts, J.A. Killian, Interfacial anchor properties of tryptophan residues in transmembrane peptides can dominate over hydrophobic matching effects in peptide-lipid interactions, Biochemistry 42 (2003) 5341–5348.
[40] E.L. Ulrich, H. Akutsu, J.F. Doreleijers, Y. Harano, Y.E. Ioannidis, J. Lin, M. Livny, S. Mading, D. Maziuk, Z. Miller, E. Nakatani, C.F. Schulte, D.E. Tolmie, R. K. Wenger, H.Y. Yao, J.L. Markley, BioMagResBank, Nucleic Acids Res. 35 (2007) D402–D408.
[41] S. Li, M. Hong, Protonation, tautomerization, and rotameric structure of histidine: a comprehensive study by magic-angle-spinning solid-state NMR, J. Am. Chem. Soc. 133 (2011) 1534–1544.
[42] D.P. Raleigh, M.H. Levitt, R.G. Griffin, Rotational resonance in solid state NMR, Chem. Phys. Lett. 146 (1988) 71–76.
[43] C.R. Morcombe, K.W. Zilm, Chemical shift referencing in MAS solid state NMR, J. Magn. Reson. 162 (2003) 479–486.
[44] M. Hong, R.G. Griffin, Resonance assignment for solid peptides by dipolar-mediated $^{13}C/^{15}N$ correlation solid-state NMR, J. Am. Chem. Soc. 120 (1998) 7113–7114.
[45] C.M. Rienstra, L. Tucker-Kellogg, C.P. Jaroniec, M. Hohwy, B. Reif, M. T. McMahon, B. Tidor, T. Lozano-Perez, R.G. Griffin, De novo determination of peptide structure with solid-state magic-angle spinning NMR spectroscopy, Proc. Natl. Acad. Sci. USA 99 (2002) 10260–10265.
[46] W.T. Franks, D.H. Zhou, B.J. Wylie, B.G. Money, D.T. Graesser, H.L. Frericks, G. Sahota, C.M. Rienstra, Magic-angle spinning solid-state nmr spectroscopy of the b1 immunoglobulin binding domain of protein G (GB1): ^{15}N and ^{13}C chemical shift assignments and conformational analysis, J. Am. Chem. Soc. 127 (2005) 12291–12305.
[47] T. Wang, J.K. Williams, K. Schmidt-Rohr, M. Hong, Relaxation-compensated difference spin diffusion NMR for detecting $^{13}C–^{13}C$ long-range correlations in proteins and polusaccharides, J. Biomol. NMR 61 (2014) 97–107.
[48] S. Li, Y. Zhang, M. Hong, 3D $^{13}C–^{13}C–^{13}C$ correlation NMR for de novo distance determination of solid proteins and application to a human alpha defensin, J. Magn. Reson. 202 (2010) 203–210.